Bulletin of Volcanology (2018) 80: 71
https://doi.org/10.1007/s00445-018-1244-y

RESEARCH ARTICLE

Relationship between infrasound-derived and buoyancy-derived eruption plume volume estimates

Taishi Yamada[1] · Hiroshi Aoyama[2] · Hideki Ueda[1]

Received: 16 March 2018 / Accepted: 3 August 2018 / Published online: 16 August 2018
© Springer-Verlag GmbH Germany, part of Springer Nature 2018

Abstract

Volume estimations for discrete plumes accompanying short-lived eruptions are potentially possible using infrasound signals. Plumes emitted during short-lived (discrete) eruptions have been modeled as discrete thermals or rooted thermals. Based on the one-dimensional model for the rise of a discrete thermal, the initial buoyancy, F_0, of a spherical thermal can theoretically be estimated from the maximum plume height and a vertical profile of ambient air density. We here examine the relationship between infrasound-derived volume, V_{inf}, and the buoyancy-derived volume, V_b, as derived from F_0, which depends on gravity acceleration, and the difference in density between the thermal and surrounding air, to understand how V_{inf} relates to the dynamics of the eruption plume. We analyze infrasound data accompanying Vulcanian and phreatic eruptions at Aso, Shinmoedake, and Lokon-Empung volcanoes to estimate V_{inf}, and consider V_{inf} from other volcanoes. We obtain a representative ratio of V_b/V_{inf} of 16 by examining 53 events. Because the analyzed infrasound signals share a prominent pressure pulse at the onset, we regard V_{inf} as the volume of the plume at initiation, i.e., as a jet. Instead, we consider V_b as the thermal volume when it has entrained a sufficient amount of the surrounding air and obtains F_0. Comparison of the bulk density of the jet and the discrete thermal yields a rate of volume change between both regimes by a factor of 1.8–32, which is consistent with the ratio of V_b/V_{inf}. Our result provides an effective index to constrain erupted plume volume using infrasound data with real-time monitoring systems.

Keywords Volcanic infrasound · Eruption plume · Thermal · Vulcanian eruption

Introduction

Infrasound observation at active volcanoes has played an important role in monitoring volcanic activity and understanding eruption dynamics (e.g., Vergniolle and Brandeis 1994; Ripepe et al. 2001; Ripepe and Marchetti 2002; Dabrowa et al. 2011; Fee et al. 2013). Volcanic infrasound signals vary in amplitude, duration, and peak frequency, which reflects the diversity of eruption styles and dynamics at the acoustic source (e.g., Johnson and Ripepe 2011; Fee and Matoza 2013; Marchetti et al. 2009). The characteristics of infrasound records accompanying intermittent Strombolian eruptions are well explained based on the model of vibration and burst of a bubble (Vergniolle and Brandeis 1996; Vergniolle and Caplan-Auerbach 2004; Vidal et al. 2006). Attempts at acoustic source quantification has also been made with acoustic power (Vergniolle et al. 2004) and by applying a monopole source assumption (Johnson et al. 2004). Previous works focusing on small-scale gas-rich (Strombolian) eruptions have demonstrated that infrasound waveform analysis can be used to estimate gas volumes, which give results comparable to those obtained by other observation methods (e.g., Oshima and Maekawa 2001; Dalton et al. 2010; Delle Donne et al. 2016). Vulcanian eruptions, which are more explosive than the Strombolian type, yield an infrasound "pulse signal" (e.g., Petersen et al. 2006; Yokoo et al. 2009; Firstov et al. 2013). Such a pressure pulse has also been explained by volume change of a monopole source assumed to be located at the vent (Johnson and Miller 2014). Instead, the source of infrasound signals accompanying stronger, steady emission events (such as Plinian eruptions) is usually modeled as a dipole (Vergniolle

Editorial responsibility: S. Vergniolle

✉ Taishi Yamada
taishi@bosai.go.jp

[1] National Research Institute for Earth Science and Disaster Resilience, 3-1, Tennodai, Tsukuba, Ibaraki 3050006, Japan

[2] Graduate School of Science, Institute of Seismology and Volcanology, Hokkaido University, Kita 10, Nishi 8, Kita-ku, Sapporo 0600810, Japan

and Caplan-Auerbach 2006) or turbulent jet noise (Matoza et al. 2009). In case a monopole source is adopted, the inferred volume, V_{inf}, is considered to be equivalent to that of the mixture of hot volcanic particles and gases emerging from the vent that displace the atmosphere above the vent. For events having an eruption cloud with a height of the order of several kilometers, previous studies have reported that V_{inf} is considerably smaller than the video-derived volume, V_{video} (Johnson and Miller 2014; Yamada et al. 2017). A possible explanation of the cause of the discrepancy is the entrainment of surrounding air into the eruption cloud, which is not taken into account in the analyses based upon the monopole assumption. As a result, assuming that V_{inf} is the volume of the total eruption cloud appears to be inadequate. However, since the infrasound data can be obtained in real time as part of an operational monitoring system, a simple waveform analysis with the monopole assumption remains an effective and efficient method to approximately quantify the acoustic source in near-real time and immediately after the eruption. Therefore, it is important to understand how V_{inf} relates eruption cloud volume and its component parts.

An eruption cloud accompanying a short-lived eruption is usually modeled as a thermal (e.g., Turner 1962; Woods and Kienle 1994; Sparks et al. 1997). Terada and Ida (2007) revealed that the kinematic features of volcanic clouds accompanying short-lived eruptions can be explained by assuming that the cloud is an isolated spherical thermal. A simple method proposed by Terada and Ida (2007) allows initial buoyancy of the thermal, F_0, to be estimated with the maximum cloud height and a vertical profile of ambient air density without considering thermodynamics. Here, F_0 is given by the product of the volume of the thermal, V_b, gravity acceleration, and the difference in density between the thermal and the ambient air. The thermal is expected to obtain F_0 when it has entrained enough of the surrounding air to ascend by buoyancy only. We focus on V_b at that moment of transition to buoyancy, which can be obtained with the value of F_0. Investigating the relationship between V_b and V_{inf} can aid our understanding of the nature of V_{inf} and explain how V_{inf} can be linked to the dynamics of the eruption plume.

The present study analyzes infrasound waveforms accompanying Vulcanian and phreatic eruptions at Aso and Shinmoedake volcanoes in Japan and Lokon-Empung volcano in Indonesia (Fig. 1) to estimate V_{inf}. We also refer to data for V_{inf} estimated in previous studies (Johnson and Miller 2014; Kim et al. 2015; Fee et al. 2017; Yamada et al. 2017). Estimation of F_0 for each eruption follows the method of Terada and Ida (2007) which allow us to obtain V_b. We then examine the relationship between V_b and V_{inf} and discuss the dynamics of the eruption cloud behind the relationship.

Following Sparks et al. (1997), here we use the term "plume" to describe the explosive ejection of material from the vent. We also use the term "eruption cloud" to mean a plume which has detached from the vent. The dynamics of a short-lived explosive eruption has two main phases: gas thrust and buoyancy (e.g., Wilson and Self 1980; Patrick 2007; Marchetti et al. 2009; Chojnicki et al. 2015). Patrick (2007) describes how the gas thrust phase consists of jets and starting plumes, and how the buoyancy phase can be classified into the following two parts: rooted thermals and discrete thermals. To be consistent with Terada and Ida (2007), who examined the discrete thermals, we focus on the discrete thermal for the buoyancy phase.

Estimation of the infrasound-derived volume, V_{inf}

Dataset

Our dataset consists of 53 events, from which 22 events are available for waveform analysis (Aso, Shinmoedake, and Lokon-Empung). These include 31 events from previous studies (Johnson and Miller 2014; Kim et al. 2015; Fee et al. 2017; Yamada et al. 2017). A summary of these events is given in Table 1.

Aso volcano

Aso is an active volcano at the center of Kyusyu Island in Japan (Fig. 1b). Since December 2014, a number of Strombolian eruptions, continuous ash emission events, and phreatic eruptions have occurred (Yokoo and Miyabuchi 2015). Yamada et al. (2017) estimated V_{inf} of some phreatic eruptions in 2015 and early 2016. On 7 October 2016 (all dates and times are UTC), an explosive phreatic eruption occurred and its eruption cloud reached an altitude of 12 km (Sato et al. 2018). Infrasound signals accompanying the eruption were recorded by the observation networks of the National Institute of Earth Science and Disaster Resilience (NIED) and the Japan Metrological Agency (JMA) (Fig. 1d). The NIED operates four permanent monitoring stations at horizontal distances from the active crater ranging from 3.7 to 6.9 km. Each station has a microbarometer (AP-270, Setra) with a flat response at DC–100 Hz. The data is digitized with a sampling frequency of 1 Hz. Station ASO2 of the JMA has an infrasound microphone (ACO 3348, Aco) that has a flat response at 0.1–100 Hz with a sampling frequency of 100 Hz. Figure 2a shows microbarograms associated with the eruption. The amplitude of microbarograms is reduced at 1 km from the source assuming a geometric amplitude decrease (Johnson and Ripepe 2011). All waveforms in Fig. 2 are temporally co-located using the onset of the eruption signal at each station. Each microbarogram shares a prominent pulse at the onset and following a coherent time history. Since the sampling frequency of the microbarograms is 1 Hz, high-

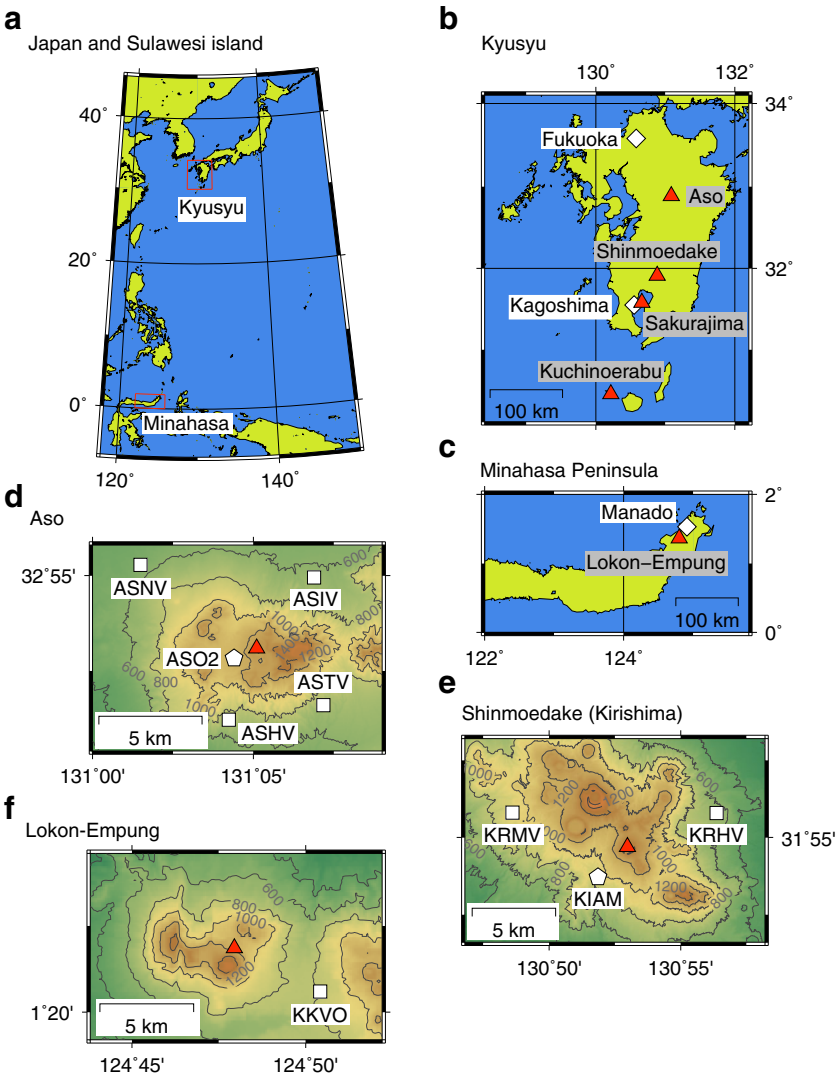

Fig. 1 **a** Map of the Pacific Ocean showing the location of Kyusyu Island (Japan) and the Minahasa Peninsula (Indonesia). Detail maps of **b** Kyusyu Island and **c** the Minahasa Peninsula, where red triangles show the location of volcanoes examined here. White diamonds denote the location of stations from which weather data were taken for the estimation of the buoyancy-derived volume, V_b. **d**, **e** Station networks at **d** Aso and **e** Shinmoedake (Kirishima volcano complex) volcanoes, where red triangles show the location of the active vents. White squares denote the stations of the NIED (ASHV, ASIV, ASTV, and ASNV at Aso and KRHV and KRMV at Shinmoedake) which has a microbarometer. The stations of the JMA (ASO2 at Aso and KIAM at Shinmoedake), that have infrasound microphones, are given by white pentagons. **f** Station map at Lokon-Empung volcano. A red triangle and a white square show the location of the active vent and the infrasound station (KKVO), respectively

frequency components (> 0.5 Hz) are not recorded in the waveforms. Figure 2d shows the reduced (at 1 km from the source) pressure waveform recorded by the microphone of the JMA, a microphone that has a flat response for the high-frequency range. Although ASO2 is located at only 1.1 km away from the active vent, the maximum amplitude of the reduced pressure waveform at ASO2 is less than half of that of the reduced microbarograms. Therefore, we consider that the contribution of the high-frequency components is not significant for the eruption signal.

Assuming the observed pressure history $\Delta P(t)$ is excited by a volumetric flow rate of $q(t)$ at a monopole source in a half-space, the relationship between $\Delta P(t)$ and $q(t)$ can be expressed by

$$\Delta P(t) = \frac{\rho_{\mathrm{atm}}}{2\pi r}\dot{q}\left(t - \frac{r}{c}\right), \qquad (1)$$

where r is the distance from the source, ρ_{atm} is the density of atmosphere near the ground (1 kg/m^3 is adopted for simplicity), and c is the sound velocity (Lighthill 1967). The relationship is valid under conditions of $r \gg \lambda/2\pi$, and $a \ll \lambda/2\pi$, where λ and a are the wavelength of the signal and a characteristic dimension of the source, respectively. In the case at Aso, the former condition seems to be valid: assuming a characteristic signal period of 10–20 s and sound velocity of 340 m/s yields $\lambda/2\pi$ of 0.5–1.3 km. However, the latter condition for the source dimension can be contentious (Johnson and Lees 2010; Johnson and Miller 2014; Yamada et al. 2017). We discuss about the possibility of failure of the compact source approximation later in this paper. Assuming that the observed pressure change satisfies Eq. 1, single and double integrations of the observed waveform yield the time histories of $q(t)$ and cumulative volume, respectively. To obtain a realistic time history by waveform integration, it is necessary to remove a linear trend from the observed waveform before integration and set an adequate integration time window. We use the method of Johnson and Miller (2014) to remove the trend from raw waveforms and to set the time window. Figure 2b, c shows the estimated time

Table 1 Summary of infrasound dataset examined in the present study

	The number of events	Event type	Observation agency	Instrument model
Aso (waveform data available)	1	Phreatic	NIED and JMA	AP-270 (Setra) and ACO3348 (Aco)
Aso (V_{inf} data referred)	4	Phreatic	NIED[a]	AP-270 (Setra) [a]
Shinmoedake (waveform data available)	9	Vulcanian	NIED and JMA	AP-270 (Setra) and ACO3348 (Aco)
Shinmoedake (V_{inf} data referred)	7	Ash emission	NIED[a]	AP-270 (Setra)[a]
Lokon-Empung (waveform data available)	12	Vulcanian	Campaign observation[b]	SI-102 (Hakusan)
Lokon-Empung (V_{inf} data referred)	4	Ash emission	Campaign observation[b]	SI-102 (Hakusan) [a,b]
Sakurajima (V_{inf} data referred)	14	Vulcanian	Campaign observation[c] Campaign observation[d,e] Campaign observation[f]	infraBSU[c] NCPA and IFS-5201 (Hyperion)[d,e] IFS-5200 (Hyperion)[f]
Kuchinoerabujima (V_{inf} data referred)	2	Phreatic	NIED[a]	PTB-100 (Vaisala)[a]

[a] Yamada et al. (2017)

[b] Yamada et al. (2016)

[c] Johnson and Miller (2014)

[d] Fee et al. (2014)

[e] Kim et al. (2015)

[f] Fee et al. (2017)

histories of $q(t)$ and the cumulative volume as obtained by integrating the observed microbarograms. The determined length of the time window (10–98 s in Fig. 2b, c) is also comparable with the duration of the short period infrasound signal at ASO2. The value of the final cumulative volume at each station is distributed within a range of 0.7–1.2 × 10^9 m^3 (Fig. 2c). At Sakurajima, Kim et al. (2015) demonstrated that the value of V_{inf} estimated by considering the effect of volcanic topography is about twice of the result which is obtained by considering a half-space medium. The contribution of signals from dipole and quadrupole sources (Woulff and McGetchin 1976) may cause the inhomogeneity of the infrasound amplitude at each station, since these sources induce an acoustic wavefield with directivity in the radiation pattern (Kim et al. 2012). The discrepancies between V_{inf} at each station may be caused by these factors. However, because we see no significant radiation pattern throughout the infrasound records, only the monopole source is assumed for the infrasound source. For simplicity, we define the average of all stations as a representative value of V_{inf}. We also attempted to estimate V_{inf} from the

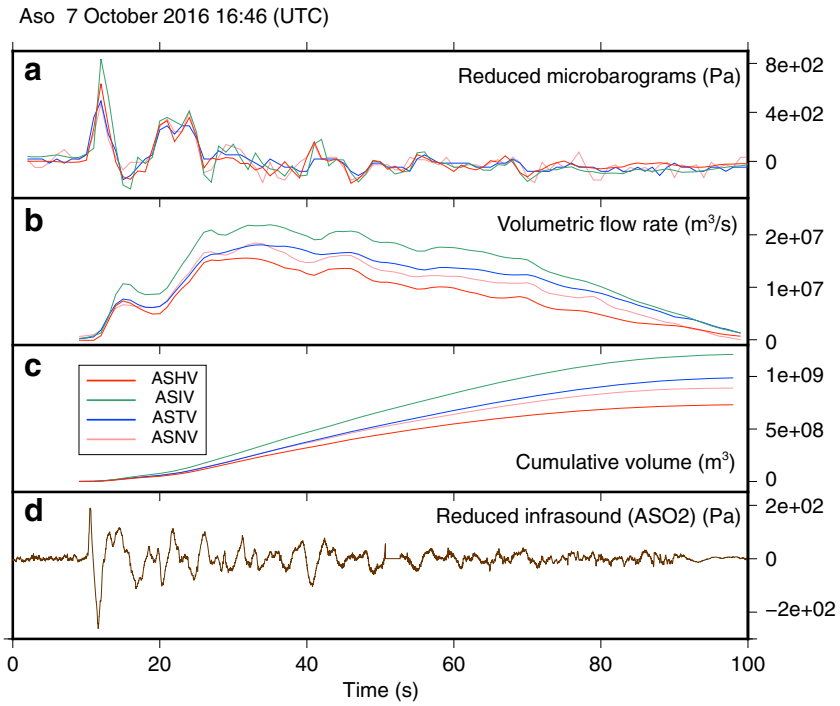

Fig. 2 **a** Reduced microbarograms (at 1 km from the source) accompanying an eruption on 7 October 2016 (16:46) at ASHV, ASIV, ASTV, and ASNV, respectively. **b** Estimated time series of volumetric flow rate, $q(t)$, at the monopole source. **c** Estimated time series of cumulative volume. **d** Reduced infrasound waveform (at 1 km from the source) at ASO2

infrasound waveform recorded by the microphone of the JMA (Fig. 2d). However, this yields a bipolar-shaped time history of $q(t)$. Since such a flux history is unrealistic for an eruption (Johnson and Miller 2014), the present study focuses on the pressure waveforms recorded by the microbarometers of the NIED only.

Shinmoedake volcano

Shinmoedake volcano is a part of the Kirishima volcanic complex in the south of Kyusyu Island (Nagaoka and Okuno 2011). It had a series of eruptions comprising three sub-Plinian eruptions, the formation of a lava dome, several Vulcanian eruptions, and continuous ash emission events in 2011 (Nakada et al. 2013). We here analyze infrasound signals accompanying nine Vulcanian eruption events that occurred during the period 28 January to 18 February 2011. In the case of continuous ash emission events, Yamada et al. (2017) estimated V_{inf} focusing on the very long period components of the infrasound signal with microbarograms recorded by the observation network of the NIED (Fig. 1e). Each station of the NIED at Shinmoedake is equipped with the same model of microbarometer with the same sampling frequency that is installed at stations on Aso. Station KIAM of the JMA also has the same microphone with a sampling frequency of 100 Hz as that at ASO2. As a representative event, reduced microbarograms accompanying a Vulcanian eruption on 31 January 2011 are shown in Fig. 3a. Both microbarograms at KRHV and KRMV show a pressure pulse with a large amplitude at the onset, which is a characteristic of an infrasound signal accompanying a Vulcanian eruption (Johnson 2003). Figure 3b, c represents the estimated time histories of the $q(t)$ and the cumulative volume at the source obtained with the same method described above. As above, we adopt the microbarograms only to estimate V_{inf} at Shinmoedake.

Lokon-Empung

Lokon-Empung volcano is an active volcano on the Minahasa Peninsula of Sulawesi island in Indonesia (Fig. 1c). During the period of September 2012 to September 2013, infrasound signals accompanying 56 Vulcanian eruption and continuous ash emission events were recorded (Yamada et al. 2016). The infrasound signals were recorded at KKVO (Fig. 1f) with a sampling frequency of 100 Hz by an infrasound microphone (SI102, Hakusan) having a flat response at 0.05–1500 Hz. We examine the signals accompanying 12 of Vulcanian eruption events which have a sufficiently high signal-to-noise ratio. Figure 4a shows the infrasound waveform associated with a Vulcanian eruption on 5 October 2012. Figure 4b, c represents the time histories of $q(t)$ and the cumulative volume estimated by the method described above. It must be considered that the infrasound waveforms at Lokon-Empung were recorded by the microphone that has a narrower flat response range than the microbarometers at Aso and Shinmoedake. The instrumental response of the microphone (SI102) is not provided analytically (Yamada et al. 2017). Therefore, no corrections are completed for infrasound waveforms at Lokon-Empung.

Sakurajima and Kuchinoerabujima

The eruption activity of Sakurajima volcano in Japan (Fig. 2b) has been characterized by numerous repeating Vulcanian eruptions since 1955 (Iguchi et al. 2013). Previous studies observed acoustic signals accompanying Vulcanian eruptions at Sakurajima (e.g., Iguchi and Ishihara 1990; Morrissey et al. 2008; Yokoo et al. 2013), and some of them have estimated V_{inf} by waveform analysis (Johnson and Miller 2014; Kim et al. 2015; Fee et al. 2017). The V_{inf} data of Kim et al. (2015) and Fee et al. (2017) was estimated by taking the effect of the volcanic topography into account.

Kuchinoerabujima is a volcanic island located at offshore of Kyusyu Island, Japan (Fig. 2b). Infrasound signals accompanying phreatic eruptions in 2014 and 2015 were recorded by two microbarometers of the NIED on the island, and V_{inf} for these eruptions were estimated using the microbarograms (Yamada et al. 2017). We here compile V_{inf} reported by these previous studies to examine the relation between V_b and V_{inf}.

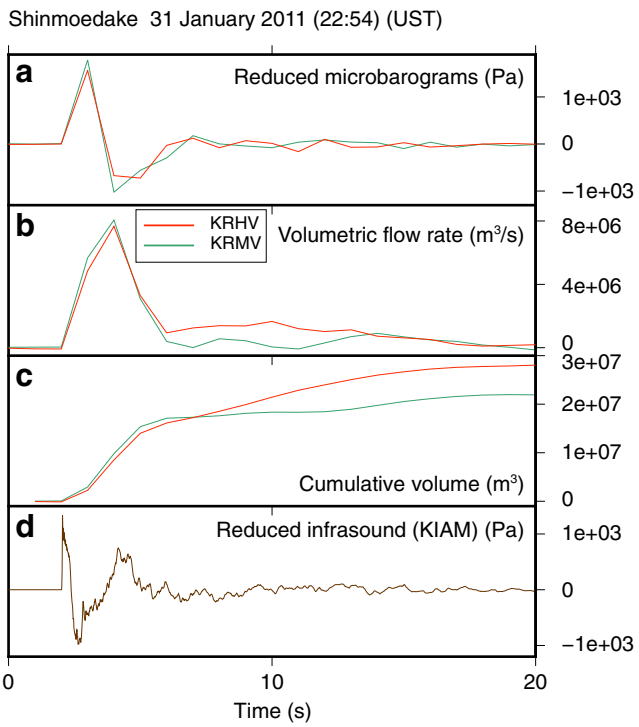

Fig. 3 **a** Reduced microbarograms (at 1 km from the source) accompanying a Vulcanian eruption on 31 January 2011 (22:54) at KRHV and KRMV. **b** Estimated time series of volumetric flow rate, $q(t)$, at the monopole source. **c** Estimated time series of cumulative volume. **d** Reduced infrasound waveform (at 1 km from the source) at KIAM

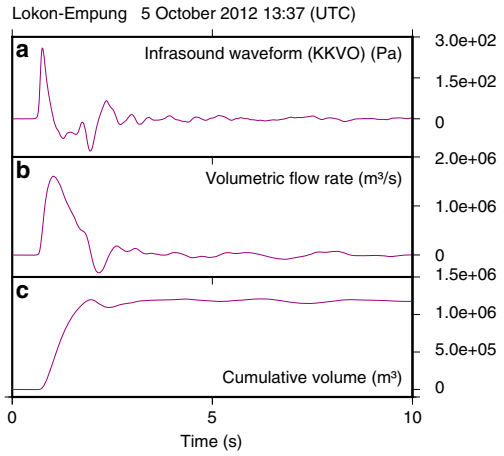

Fig. 4 **a** Raw infrasound waveform accompanying a Vulcanian eruption on 5 October 2012 (13:37) at KKVO. **b** Estimated time series of volumetric flow rate, $q(t)$, at the monopole source. **c** Estimated time series of cumulative volume

Estimation of the buoyancy-derived volume V_b

Following Terada and Ida (2007), we estimate F_0 and consequently V_b for the explosive events reviewed in the previous section. Assuming that an eruption cloud is as an isolated thermal ascending vertically with self-similarity, the radius of the thermal r spreads linearly with the height of the thermal center from the ground z_c (Woods and Kienle 1994), as

$$r = kz_c, \tag{2}$$

where k is an empirical constant (Scorer 1957). Using Eq. 2, the rate of volume change of the thermal is given by

$$\frac{\mathrm{d}}{\mathrm{d}t}\left(\frac{4}{3}\pi r^3\right) = 4\pi r^2 k w_c, \tag{3}$$

where $w_c = \mathrm{d}z_c/\mathrm{d}t$ is vertical velocity of the thermal center (Terada and Ida 2007). Equation 3 represents the volume of entrained gas through in a unit area of the thermal surface. Therefore, constant k corresponds to the entrainment constant (Morton et al. 1956). For simplicity, the present study adopts k as 0.25, which is the value obtained from laboratory experiments for a discrete thermal (Scorer 1957). The total buoyancy F of a spherical thermal is expressed as (Morton et al. 1956; Turner 1962)

$$F = \frac{4}{3}\pi r^3 g(\rho_{air} - \rho_{th}), \tag{4}$$

where g is the gravitational acceleration, ρ_{air} is the density of ambient air, and ρ_{th} is the mean density of the thermal. Using Eqs. 2 and 4, and the mass conservation of the thermal with the entrainment hypothesis (Morton et al. 1956), one obtains the equation (Terada and Ida 2007):

$$\frac{\mathrm{d}F}{\mathrm{d}z_c} = \frac{4\pi}{3} g k^3 z_c^3 \frac{\mathrm{d}\rho_{air}}{\mathrm{d}z_c}. \tag{5}$$

Integrating Eq. 5 with respect to z and adopting a vertical profile for the ambient air density, we obtain the vertical profile of F for an arbitrary initial value of F_0 at $z_c = 0$. As an example of the estimation of F_0, Fig. 5 shows the case of the eruption at Aso on 7 October 2016 (Fig. 2). Vertical profiles of the ambient air density observed at Fukuoka and Kagoshima meteorological stations of the JMA (Fig. 1b) are shown in Fig. 5a. The present study adopts the weather (pressure and temperature) data distributed by the University of Wyoming (2017). The equation of state for ambient air ($p = \rho_{air}RT$) is used to derive the ambient air density, where p is the pressure, R is the gas constant (287.05 J/kg/K), and T is the temperature of the corresponding altitude. The solid line in Fig. 5a is a quadratic least square fit for data at both Fukuoka and Kagoshima stations. With the regression of the ambient air density, vertical profiles of F for values of F_0 of 10^8–10^{11} are calculated in Fig. 5b. When the thermal reaches the neutral buoyancy height, the value of F drops sharply to 0. Figure 5c represents the relationship between the neutral buoyancy height of the thermal and the corresponding value of F_0. The height of the top of the thermal z is given by $z = z_c + r$. In the case of the eruption at Aso, the eruption cloud reached a height of 10.7 km above the crater rim. Thus, we obtain F_0 as 5.0×10^{10} for this eruption (Fig. 5c).

We use the weather data from both Fukuoka and Kagoshima stations for the events at Aso, Shinmoedake, Sakurajima, and Kuchinoerabujima volcanoes, and the data at Manado station for the events at Lokon-Empung (Fig. 1c) to estimate F_0. The data for maximum cloud height used in the analysis are summarized in Table 2. To obtain V_b ($\frac{4}{3}\pi r^3$ of Eq. 4) from the value of F_0, it is necessary to assume a difference in density between the thermal and the ambient air ($\rho_{air} - \rho_{th}$). Following Wilson and Self (1980), Woods and Kienle (1994), and Yamamoto et al. (2008), we set a value of 0.3 kg/m^3 as a characteristic density difference with an error range of ± 0.2 kg/m^3.

Results

Figure 6 shows the estimated relationship between V_b and V_{inf} for 53 events analyzed here. A correlation coefficient of 0.81 is obtained between V_b and V_{inf} for all events. The ratio of V_b/V_{inf} ranges from 0.012 to 180, with an average of 27. The ratio of V_b/V_{inf} is almost always greater than 1 (51 events) and most commonly within the range of 3–30 (33 events). In Fig. 6, we define the linear regression function between V_b and V_{inf} of 16. Because the thermal volume increases linearly with altitude, we hypothesize that the relation V_b/V_{inf} also follows the linear function. Although some events deviate from this regression,

the relationship between V_b and V_{inf} of most analyzed events roughly follows the ratio expressed by the linear regression. Table 2 summarizes the values of V_{inf}, V_b, and F_0 for each event.

Discussion

Figure 6 shows that the estimated V_{inf} is generally 3 to 30 times smaller than V_b. This is consistent with the comparison between V_{inf} and V_{video} by Johnson and Miller (2014) and Yamada et al. (2017). As we have shown in Figs. 2, 3, and 4, the analyzed infrasound waveforms exhibit a prominent compressional phase at the onset. From a perspective of the time history of observed overpressure, the estimated V_{inf} is likely to relate to the onset of plume emission which is driven by gas thrust, i.e., jets (e.g., Crapper 1977; Sparks et al. 1997; Patrick 2007). This interpretation is supported by the velocity profile with height commonly recorded for ascending plumes: rapid deacceleration in the gas thrust phase, followed by steady velocity in the buoyancy phase (e.g., Wilson and Self 1980; Patrick et al. 2007; Marchetti et al. 2009; Delle Donne and Ripepe 2012). Our interpretation is also supported by following field observation results: infrasound energy reflects the driving force of the gas thrust phase (Marchetti et al. 2009), and the duration of the gas thrust phase is highly correlated with that of infrasound signal (Delle Donne et al. 2016).

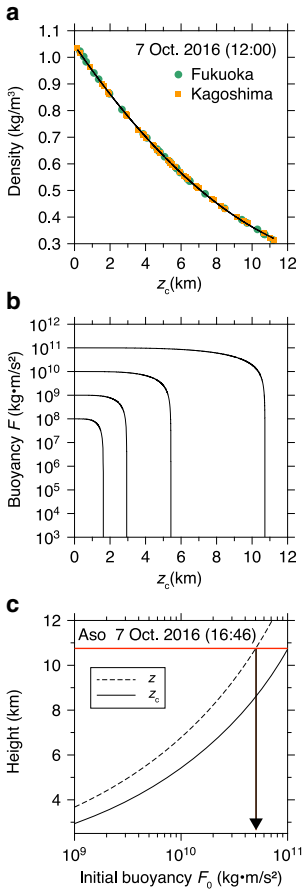

Fig. 5 **a** Vertical profiles of ambient air density at Fukuoka and Kagoshima stations on 7 October 2016 (12:00). A quadratic regression fit is given by the solid line. **b** Vertical profiles of the calculated buoyancy of the thermal F with the initial value, F_0, of 10^8–10^{11} at $z_c = 0$. **c** Neutral buoyancy height reached for a given buoyancy F_0

Because a jet barely entrains the surrounding air, where Patrick (2007) found $k = 0.06$ in the jet region of plumes at Stromboli, and Bombrun et al. (2018) estimated $k = 0.178$ at Santiaguito, the bulk density of the jet is expected to be almost the same as that of the particle-gas mixture. From the literature, the possible range of the bulk density of the jet is 2–20 kg/m^3 (e.g., Sparks and Wilson 1976; Sparks et al. 1997; Formenti et al. 2003). Fee et al. (2017) demonstrated that total eruption mass inferred from V_{inf} and the bulk density of the flow near the vent (2–5 kg/m^3) shows good agreement with that estimated from ground-based ash sampling. Therefore, we consider that V_{inf} represents the initial volume of the eruption plume driven by momentum near the vent (Fig. 7b). Since the present study focuses on short-lived eruptions, emission duration of the mixture of particles and gas from the vent is transient for each event. Hence, V_{inf} may be almost equivalent to the total emitted volume before entraining surrounding air. As it ascends from the vent, the plume gradually loses its momentum by gas thrust (Patrick et al. 2007). At the same time, the plume entrains the surrounding air and acquires buoyancy (e.g., Wilson and Self 1980; Patrick 2007; Marchetti et al. 2009). The estimated V_b can be regarded as the volume at the moment when the thermal has entrained a sufficient amount of the surrounding air to ascend by buoyancy only (Fig. 7c). Previous observations and theoretical considerations have reported the bulk density of the ascending thermal as 0.6–1.1 kg/m^3 (e.g., Wilson and Self 1980; Woods and Kienle 1994; Yamamoto et al. 2008). The difference between the bulk density of both eruption plume regimes yields 1.8–32 times of volume expansion as the plume dynamic transitions from a jet to a discrete thermal. This rate shows good agreement with the range of V_b/V_{inf} ratio of most events (3.0–30) and the regression of V_b/V_{inf} in Fig. 6 which is 16. Therefore, the ratio of V_b/V_{inf} can be explained by the rate of volume change of the eruption plume that occurs between the gas thrust and buoyant regimes.

In Fig. 6, we set error ranges for V_{inf} considering the discrepancy between the final values of the cumulative volume for each station, and for V_b considering the uncertainty of the difference in density between the thermal and the surrounding air. However, the errors derived from other factors should also be considered. The maximum eruption cloud height is an important parameter to consider in our estimate of V_b. The present study adopts data for the maximum eruption cloud height both inferred from weather radar and ground-based visual observation (Table 2). The maximum cloud height of some

Table 2 Date, V_{inf}, V_b, F_0, the maximum eruption cloud height from the ground (z_{max}), elevation of the crater rim (z_0), and date of weather data for each event

	Date	V_{inf} (m^3)	V_b (m^3)	F_0 (N)	z_{max} (km)	z_0 (km)	Weather date
Aso	15 September 2015 (00:43)	2.5×10^7 [a]	3.6×10^7	1.0×10^8	3.2[b]	1.2	15 September 2015 (00:00)
	22 October 2015 (17:00)	4.9×10^6 [a]	8.8×10^6	2.6×10^7	2.6[c]	1.2	22 October 2015 (12:00)
	6 December 2015 (23:11)	6.6×10^5 [a]	3.4×10^5	1.0×10^6	1.9[c]	1.2	7 December 2015 (00:00)
	18 February 2016 (07:57)	1.2×10^6 [a]	1.6×10^7	4.9×10^7	2.8[d]	1.2	18 February 2016 (12:00)
	7 October 2016 (16:46)	$9.5 \pm 2.2 \times 10^8$	1.7×10^{10}	5.0×10^{10}	10.7[e]	1.2	7 October 2016 (12:00)
Shinmoedake	27 January 2011 (06:41)	1.3×10^8 [a]	1.0×10^9	3.0×10^9	4.9[f]	1.3	27 January 2011 (12:00)
	28 January 2011 (03:47)	$7.5 \pm 0.6 \times 10^7$	3.7×10^8	1.1×10^9	3.6[f]	1.3	28 January 2011 (00:00)
	31 January 2011 (22:54)	$2.5 \pm 3.4 \times 10^7$	1.9×10^9	5.6×10^9	5.6[f]	1.3	1 February 2011 (00:00)
	1 February 2011 (14:19)	2.9×10^7 [a]	6.8×10^8	2.0×10^9	4.3[f]	1.3	1 February 2011 (12:00)
	1 February 2011 (20:25)	$7.2 \pm 2.2 \times 10^7$	1.7×10^9	5.6×10^9	5.4[f]	1.3	2 February 2011 (00:00)
	2 February 2011 (03:47)	$6.6 \pm 0.0 \times 10^7$	4.7×10^8	1.4×10^9	3.8[f]	1.3	2 February 2011 (00:00)
	2 February 2011 (06:53)	$4.7 \pm 1.1 \times 10^7$	8.8×10^8	2.6×10^9	4.6[f]	1.3	2 February 2011 (12:00)
	2 February 2011 (23:09)	2.6×10^6 [a]	3.4×10^8	1.0×10^9	4.2[f]	1.3	3 February 2011 (00:00)
	4 February 2011 (00:42)	$1.4 \pm 0.1 \times 10^8$	2.8×10^9	8.4×10^9	6.3[f]	1.3	4 February 2011 (00:00)
	5 February 2011 (18:16)	2.7×10^7 [a]	3.4×10^8	1.0×10^9	3.7[f]	1.3	6 February 2011 (00:00)
	6 February 2011 (21:07)	1.8×10^7 [a]	3.5×10^7	1.0×10^8	3.3[f]	1.3	7 February 2011 (00:00)
	11 February 2011 (02:36)	$1.0 \pm 0.0 \times 10^8$	3.7×10^8	1.1×10^9	3.6[f]	1.3	11 February 2011 (00:00)
	13 February 2011 (20:07)	$1.6 \pm 0.0 \times 10^8$	6.9×10^9	2.0×10^{10}	8.0[f]	1.3	14 February 2011 (00:00)
	18 February 2011 (09:16)	$1.9 \pm 0.0 \times 10^8$	4.4×10^8	1.3×10^9	3.8[f]	1.3	18 February 2011 (12:00)
	13 March 2011 (08:45)	3.5×10^8 [a]	2.3×10^9	7.0×10^9	6.2[f]	1.3	13 March 2011 (12:00)
	2 April 2011 (23:41)	2.5×10^7 [a]	3.4×10^8	1.0×10^9	4.1[f]	1.3	3 April 2011 (00:00)
Lokon-Empung	5 October 2012 (13:37)	7.5×10^6	1.0×10^7	3.1×10^7	2.5[g]	1.0	5 October 2012 (12:00)
	26 November 2012 (03:17)	4.3×10^5 [a]	7.8×10^7	2.3×10^8	2.5[g]	1.0	26 November 2012 (00:00)
	28 November 2012 (02:05)	9.1×10^6 [a]	2.8×10^8	8.5×10^8	3.5[g]	1.0	28 November 2012 (00:00)
	1 December 2012 (08:11)	1.8×10^6	7.8×10^7	2.3×10^8	3.5[g]	1.0	1 December 2012 (12:00)
	3 December 2012 (07:42)	4.8×10^6	4.7×10^8	1.4×10^9	5.0[g]	1.0	3 December 2012 (12:00)
	6 December 2012 (09:18)	1.5×10^6	2.9×10^8	8.6×10^9	4.5[g]	1.0	6 December 2012 (09:18)
	8 December 2012 (15:01)	2.8×10^5 [a]	7.8×10^7	2.3×10^8	2.5[g]	1.0	8 December 2012 (12:00)
	11 December 2012 (04:09)	3.2×10^6	1.5×10^8	4.7×10^8	4.0[g]	1.0	11 December 2012 (00:00)
	8 January 2013 (01:49)	1.9×10^6	8.1×10^7	2.4×10^8	3.5[g]	1.0	8 January 2013 (00:00)
	16 January 2013 (11:39)	7.5×10^6 [a]	2.8×10^8	8.5×10^8	3.5[g]	1.0	16 January 2013 (12:00)
	4 February 2013 (16:54)	4.1×10^6	7.8×10^7	2.3×10^8	3.5[g]	1.0	4 February 2013 (12:00)
	19 March 2013 (23:54)	8.1×10^6	3.4×10^7	1.0×10^8	3.0[g]	1.0	20 March 2013 (00:00)
	24 March 2013 (21:10)	2.0×10^6	3.0×10^7	9.0×10^7	3.0[g]	1.0	25 March 2013 (00:00)
	8 April 2013 (01:57)	1.5×10^6	1.6×10^8	4.8×10^8	4.0[g]	1.0	8 April 2013 (00:00)
	11 April 2013 (02:51)	1.6×10^6	3.4×10^7	1.0×10^8	3.0[g]	1.0	11 April 2013 (00:00)
	8 September 2013 (22:34)	9.3×10^6	1.1×10^7	3.2×10^7	2.5[g]	1.0	9 September 2013 (00:00)
Sakurajima	19 July 2013 (02:19)	0.8×10^6 [h]	1.0×10^7	3.0×10^7	2.4[k]	0.9	19 July 2013 (00:00)
	19 July 2013 (03:04)	8.3×10^6 [h]	1.6×10^8	4.8×10^8	3.9[k]	0.9	19 July 2013 (00:00)
	19 July 2013 (09:52)	0.2×10^6 [h]	3.4×10^6	1.0×10^7	2.2[k]	0.9	19 July 2013 (12:00)
	19 July 2013 (10:50)	8.4×10^6 [h]	6.8×10^7	2.0×10^8	3.3[k]	0.9	19 July 2013 (12:00)
	20 July 2013 (03:11)	6.9×10^6 [h]	6.8×10^7	2.0×10^8	3.3[k]	0.9	20 July 2013 (00:00)
	20 July 2013 (07:12)	4.2×10^6 [h]	9.1×10^7	2.7×10^8	3.5[k]	0.9	20 July 2013 (12:00)
	20 July 2013 (22:33)	3.0×10^6 [i]	6.4×10^7	1.9×10^8	3.3[k]	0.9	21 July 2013 (00:00)
	21 July 2013 (00:55)	5.2×10^6 [h]	3.0×10^7	9.0×10^7	2.9[k]	0.9	21 July 2013 (00:00)
	21 July 2013 (02:22)	1.8×10^6 [h]	2.0×10^7	6.0×10^7	2.7[k]	0.9	21 July 2013 (00:00)
	21 July 2013 (05:04)	3.5×10^6 [h]	5.4×10^7	1.6×10^8	3.2[k]	0.9	21 July 2013 (00:00)
	12 February 2015 (02:11)	1.7×10^6 [j]	2.0×10^6	6.0×10^6	1.9[l]	0.9	12 February 2015 (00:00)

Table 2 (continued)

	Date	V_{inf} (m^3)	V_b (m^3)	F_0 (N)	z_{max} (km)	z_0 (km)	Weather date
	13 February 2015 (07:32)	1.1×10^6 [j]	7.1×10^6	2.1×10^7	2.2[l]	0.9	13 February 2015 (12:00)
	14 February 2015 (03:48)	6.2×10^6 [j]	4.0×10^7	1.2×10^8	2.9[l]	0.9	14 February 2015 (00:00)
	15 February 2015 (08:28)	7.2×10^6 [j]	4.4×10^7	1.3×10^8	3.0[l]	0.9	15 February 2015 (12:00)
Kuchinoerabujima	3 August 2014 (03:24)	5.5×10^7 [a]	6.8×10^5	2.0×10^6	1.4[m]	0.6	3 August 2014 (00:00)
	29 May 2015 (00:59)	6.4×10^8 [a]	1.2×10^{10}	3.8×10^{10}	9.8[n]	0.6	29 May 2015 (00:00)

[a] Yamada et al. (2017)
[b] JMA (2018a)
[c] JMA (2018b)
[d] JMA (2018c)
[e] Sato et al. (2018)
[f] Shimbori et al. (2013)
[g] Eruption list by KKVO (ground-based visual observation)
[h] Johnson and Miller (2014)
[i] Kim et al. (2015)
[j] Fee et al. (2017)
[k] JMA (2013)
[l] JMA (2015a)
[m] JMA (2016)
[n] JMA (2015b)

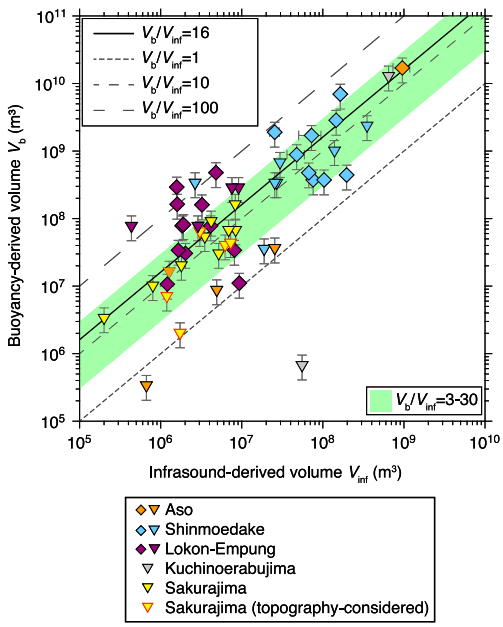

Fig. 6 Relationship between the infrasound-derived volume, V_{inf}, and the buoyancy-derived volume, V_b. The events represented by diamonds express the relation between V_{inf} and V_b. These events have a horizontal error bar defined by uncertainty in V_{inf} at each station. Inverted triangles are events for which only V_b is estimated here, but for which the value of V_{inf} is taken from other studies (Johnson and Miller 2014; Kim et al. 2015; Fee et al. 2017; Yamada et al. 2017). Vertical error bars for all events correspond to uncertainty in V_b based on the value of $(\rho_{air} - \rho_{th})$ which has an error range of ± 0.2 kg/m^3. Some events at Sakurajima (as outlined by the red box) have V_{inf} estimated considering the effect of topography (Kim et al. 2015; Fee et al. 2017). The solid regression line shows that $V_b/V_{inf} = 16$. Dashed lines represent the V_b/V_{inf} ratio of 1, 10, and 100

events at Shinmoedake was estimated by both methods: weather radar (Shimbori et al. 2013) and visual observation (Kato and Yamasato 2013). For example, for an event on 2 January 2011 (06:53), the weather radar detected the maximum eruption cloud height as 4.6 km above the crater (Shimbori et al. 2013). On the other hand, the visual observation from the ground estimated the maximum cloud height as 3.0 km above the crater (Kato and Yamasato 2013). If we adopt the maximum height data by the ground-based visual observation, this yields a value of V_b that is 4.8 times smaller than that estimated by the weather radar data. Such an error derived from the differences in estimation of cloud height is included in our results. The maximum cloud height is usually affected by several factors, such as the wind (Bursik 2001) and the total grain-size distribution (Girault et al. 2014). For example, the event at Kuchinoerabujima volcano in 2014 (V_{inf} =

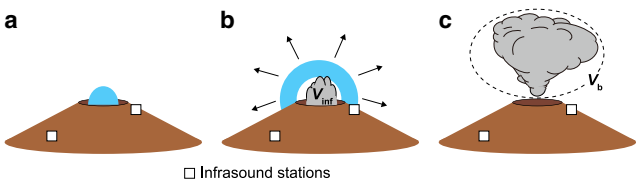

Fig. 7 Schematic illustration of the plume volume inferred in the present study. **a** Before an eruption, where the atmosphere, denoted by the blue dome, corresponds to the volume that will be displaced by the emerging jet. **b** At the onset of the eruption, the plume is driven by gas thrust where the jet displaces the atmosphere and induces an infrasound pulse observed at the surrounding stations. V_{inf} corresponds to the volume of the jet. **c** The eruption cloud entrains surrounding air and obtains buoyancy. V_b corresponds to the volume of the plume at that moment

5.5×10^7 m^3, $V_b = 6.8 \times 10^5$ m^3) deviates considerably from the trend of most of the events represented by the regression line in Fig. 6. Iguchi and Nakamichi (2015) reported that strong wind from a nearby typhoon affected the maximum plume height of this eruption. The value of F_0 and V_b may also be overestimated if the eruption plume overshoots the neutral buoyancy height (Holasek and Self 1995). Another critical parameter for estimation of V_b is the entrainment constant, k. It is known that this value can be affected by the interaction between an eruption plume and wind in the atmosphere (Suzuki and Koyaguchi 2015). Although there are theoretical models that consider the effect of wind on entrainment (Bursik 2001), quantification of the wind effect is still challenging even for recent numerical simulation models (Costa et al. 2016). Jessop and Jellinek (2014) reported that vent geometry modifies the shape of eddies on the edge of the plume and, thus, can affect entrainment of the ambient air. Although most previous studies have demonstrated that k can be considered as a constant approximately, Carazzo et al. (2008) pointed out that a better fit for experimental data is obtained setting k as a function of buoyancy. Terada and Ida (2007) determined k from video image analyses and reported that k varies in the range of 0.22–0.59. Bombrun et al. (2018) inferred k of a rooted thermal at Santiaguito as 0.356 from an analysis of thermal video images. For example, if we adopt k as 0.36, the average value from Terada and Ida (2007), V_b of the event at Aso (Fig. 2) becomes 1.1×10^{11} m^3, i.e., 2.2 times greater than that obtained by setting k at 0.25. The linear regression function for the V_b/V_{inf} ratio of all events with k as 0.36 becomes 34, where it is also similar to the rate of volume change expected from the transition of the eruption plume regime.

The assumption of the compact source adopted in the estimation of V_{inf} may not be adequate for some events. The waveform analysis of the event at Aso examined in Fig. 2 yields V_{inf} as 9.5×10^8 m^3. Assuming that the eruption cloud is a sphere, the radius of the sphere is 0.61 km. For infrasound signal with periods of 10–20 s and a sound velocity of 340 m/s, the source dimension is no longer compact relative to the value of $\lambda/2\pi$ of 0.5–1.3 km. This issue is a challenging topic for the study of volcanic infrasound and may be solved with detailed analysis techniques, such as the superposition of multiple monopole sources discussed by Johnson and Lees (2010). The present study compiles V_{inf} of some events that are estimated by considering the effect of volcanic topography, which affects the estimation of V_{inf} on the order of two times reported by Kim et al. (2015). However, we see no significant difference between topography-considered and half-space-considered events in our result in Fig. 6. Since we focus on the macroscopic scale over several orders of magnitude, it seems that the effect of volcanic topography is not influential in our results. However, accounting for topography in the infrasound analysis will be necessary for accurate estimation of V_{inf} and for examining plume dynamics at a more detailed scale.

Although our results contain unresolved errors, we consider that they are representative of the macroscopic dynamics of an eruption plume emitted during a short-lived eruption: the rate of volume change of the plume as it transitions from gas thrust-driven to buoyancy-driven regimes appears valid. The estimated relationship between V_{inf} and V_b can also be of value in constraining the volume of plume with infrasound data. The maximum plume height can also be constrained with our method if the vertical profile of the ambient air density is available.

Conclusions

We have here examined the relationship between infrasound-waveform-derived eruption plume volume, V_{inf}, and the buoyancy-derived plume volume, V_b, obtained by considering plume as a discrete thermal. The infrasound waveforms accompanying short-lived (Vulcanian and phreatic) eruptions at Aso, Shinmoedake, and Lokon-Empung volcanoes were analyzed to estimate V_{inf}. We also referred to values of V_{inf} reported by previous studies at several other volcanoes. The estimation of V_b followed the method of Terada and Ida (2007) which uses the maximum eruption cloud height and a vertical profile of the ambient air density. Estimated relationships of V_b/V_{inf} for most events are in the range of 3–30, and we obtain a ratio of V_b to V_{inf} of 16. This ratio can be explained by the rate of volume change of the eruption plume as it transitions from a jet regime to that of a discrete thermal. The relationship can be a valuable index to estimate the eruption cloud volume with infrasound data. Since infrasound data can be obtained in real time at appropriately configured monitoring systems, the V_b/V_{inf} relation can be useful in assessing the magnitude of the eruption immediately after the onset of the event. Real-time provision of V_b and F_0 inferred from V_{inf} will also be useful in forecasting ash fall (Bonadonna et al. 2005).

Acknowledgements TY acknowledges A. Terada, M. Iguchi, H. Nakamichi, Y. J. Suzuki, and Y. Iriyama for having valuable discussions. We appreciate Japan Meteorological Agency (Tokyo) for providing infrasound data, and the Geospatial Information Authority of Japan (Tsukuba) for providing topographic data at Aso and Shinmoedake volcanoes. Infrasound observation at Lokon-Empung was supported by Kakaskasen Volcano Observatory (Tomohon) and the Center for Volcanology and Geological Hazard Mitigation (Bandung) in Indonesia. Topographic data at Lokon-Empung was obtained from SRTM-3 (http://dds.cr.usgs.gov/srtm/version2_1). Careful reviews by two anonymous reviewers and comments from the AE, Sylvie Vergniolle, and the EE, Andrew Harris, significantly improved the quality of the manuscript.

Funding information The present study was partly supported by the Ministry of Education, Culture, Sports, Science, and Technology (MEXT) of Japan, under its Earthquake and Volcano Hazards Observation and Research Program, Integrated Program for Next Generation Volcano Research and Human Resource Development, and JSPS KAKENHI Grant Number JP17H07345.

References

Bombrun M, Jessop D, Harris A, Barra V (2018) An algorithm for the detection and characterisation of volcanic plumes using thermal camera imagery. J Volcanol Geotherm Res 352:26–37. https://doi.org/10.1016/j.jvolgeores.2018.01.006

Bonadonna C, Connor CB, Houghton BF et al (2005) Probabilistic modeling of tephra dispersal: hazard assessment of a multiphase rhyolitic eruption at Tarawera, New Zealand. J Geophys Res Solid Earth 110:1–21. https://doi.org/10.1029/2003JB002896

Bursik M (2001) Effect of wind on the rise height of volcanic plumes. Geophys Res Lett 28:3621–3624. https://doi.org/10.1029/2001GL013393

Carazzo G, Kaminski E, Tait S (2008) On the rise of turbulent plumes: quantitative effects of variable entrainment for submarine hydrothermal vents, terrestrial and extra terrestrial explosive volcanism. J Geophys Res Solid Earth 113:B09201. https://doi.org/10.1029/2007JB005458

Chojnicki KN, Clarke AB, Phillips JC, Adrian RJ (2015) The evolution of volcanic plume morphology in short-lived eruptions. Geology 43:707–710. https://doi.org/10.1130/G36642.1

Costa A, Suzuki YJ, Cerminara M, Devenish BJ, Ongaro TE, Herzog M, van Eaton AR, Denby LC, Bursik M, de' Michieli Vitturi M, Engwell S, Neri A, Barsotti S, Folch A, Macedonio G, Girault F, Carazzo G, Tait S, Kaminski E, Mastin LG, Woodhouse MJ, Phillips JC, Hogg AJ, Degruyter W, Bonadonna C (2016) Results of the eruptive column model inter-comparison study. J Volcanol Geotherm Res 326:2–25. https://doi.org/10.1016/j.jvolgeores.2016.01.017

Crapper P (1977) Forced plume characteristics. Tellus 29:470–475. https://doi.org/10.3402/tellusa.v29i5.11380

Dabrowa AL, Green DN, Rust AC, Phillips JC (2011) A global study of volcanic infrasound characteristics and the potential for long-range monitoring. Earth Planet Sci Lett 310:369–379. https://doi.org/10.1016/j.epsl.2011.08.027

Dalton MP, Waite GP, Watson IM, Nadeau PA (2010) Multiparameter quantification of gas release during weak Strombolian eruptions at Pacaya Volcano, Guatemala. Geophys Res Lett 37:L09303. https://doi.org/10.1029/2010GL042617

Delle Donne D, Ripepe M (2012) High-frame rate thermal imagery of strombolian explosions: implications for explosive and infrasonic source dynamics. J Geophys Res Solid Earth 117:B09206. https://doi.org/10.1029/2011JB008987

Delle Donne D, Ripepe M, Lacanna G, Tamburello G, Bitetto M, Aiuppa A (2016) Gas mass derived by infrasound and UV cameras: implications for mass flow rate. J Volcanol Geotherm Res 325:169–178. https://doi.org/10.1016/j.jvolgeores.2016.06.015

Fee D, Matoza R (2013) An overview of volcano infrasound: from Hawaiian to Plinian, local to global. J Volcanol Geotherm Res 249:123–139. https://doi.org/10.1016/j.jvolgeores.2012.09.002

Fee D, McNutt SR, Lopez TM et al (2013) Combining local and remote infrasound recordings from the 2009 Redoubt Volcano eruption. J Volcanol Geotherm Res 259:100–114. https://doi.org/10.1016/j.jvolgeores.2011.09.012

Fee D, Yokoo A, Johnson JB (2014) Introduction to an open community infrasound dataset from the actively erupting Sakurajima Volcano, Japan. Seismol Res Lett 85:1151–1162. https://doi.org/10.1785/0220140051

Fee D, Izbekov P, Kim K, Yokoo A, Lopez T, Prata F, Kazahaya R, Nakamichi H, Iguchi M (2017) Eruption mass estimation using infrasound waveform inversion and ash and gas measurements: evaluation at Sakurajima Volcano, Japan. Earth Planet Sci Lett 480:42–52. https://doi.org/10.1016/j.epsl.2017.09.043

Firstov PP, Fee D, Makhmudov ER (2013) The explosive activity of Karymskii Volcano, Kamchatka: Acoustic and seismic observations. J Volcanol Seismol 7(4):252–264

Formenti Y, Druitt TH, Kelfoun K (2003) Characterisation of the 1997 Vulcanian explosions of Soufrière Hills Volcano, Montserrat, by video analysis. Bull Volcanol 65:587–605. https://doi.org/10.1007/s00445-003-0288-8

Girault F, Carazzo G, Tait S, Ferrucci F, Kaminski É (2014) The effect of total grain-size distribution on the dynamics of turbulent volcanic plumes. Earth Planet Sci Lett 394:124–134. https://doi.org/10.1016/j.epsl.2014.03.021

Holasek RE, Self S (1995) GOES weather satellite observations and measurements of the May 18, 1980, Mount St. Helens eruption. J Geophys Res Solid Earth 100:8469–8487. https://doi.org/10.1029/94jb03137

Iguchi M, Ishihara K (1990) Comparison of earthquakes and air-shocks accompanied with explosive eruptions at Sakurajima and Suwanosejima volcanoes. Annu Disaster Prev Res Inst Kyoto Univ 33B-1:1–12 (in Japanese with English abstract)

Iguchi M, Nakamichi H (2015) Successive occurrence of phreatic eruptions in Japan. Annu Disaster Prev Res Inst Kyoto Univ 58A:1–7 (in Japanese with English abstract)

Iguchi M, Tameguri T, Ohta Y et al (2013) Characteristics of volcanic activity at Sakurajima volcanos Showa crater during the period 2006 to 2011. Bull Volcanol Soc Japan 58:115–135

Japan Meteorological Agency (2013) Eruption list of Sakurajima volcano in 2013. Jpn Meteorol Agency, Kagoshima, Accessed 11 December, 2017 http://www.jma-net.go.jp/kagoshima/vol/data/skr_exp_2013.html (in Japanese)

Japan Meteorological Agency (2015a) Eruption list of Sakurajima volcano in 2015. Jpn Meteorol Agency, Kagoshima, Accessed 11 December, 2017 http://www.jma-net.go.jp/kagoshima/vol/data/skr_exp_2015.html (in Japanese)

Japan Meteorological Agency (2015b) Kuchinoerabujima, paper presented at special meeting of Coordinating Committee for Prediction of Volcanic Eruptions. Japan Meteorological Agency, Tokyo, Accessed 27 July 2018 https://www.data.jma.go.jp/svd/vois/data/tokyo/STOCK/kaisetsu/CCPVE/CCPVE08.html (in Japanese)

Japan Meteorological Agency (2016) Report of Coordinating Committee for Prediction of Volcanic Eruption No. 119. Jpn Meteorol Agency, Tokyo, Accessed 27 July 2018 https://www.data.jma.go.jp/svd/vois/data/tokyo/STOCK/kaisetsu/CCPVE/Report/ccpve_bulletin_119.html (in Japanese)

Japan Meteorological Agency (2018a) Report of Coordinating Committee for Prediction of Volcanic Eruption No.122. Jpn Meteorol Agency, Tokyo, Accessed 27 July 2018 https://www.data.jma.go.jp/svd/vois/data/tokyo/STOCK/kaisetsu/CCPVE/Report/ccpve_bulletin_122.html (in Japanese)

Japan Meteorological Agency (2018b) Report of Coordinating Committee for Prediction of Volcanic Eruption No.123. Jpn Meteorol Agency, Tokyo, Accessed 27 July 2018 https://www.data.jma.go.jp/svd/vois/data/tokyo/STOCK/kaisetsu/CCPVE/Report/ccpve_bulletin_123.html (in Japanese)

Japan Meteorological Agency (2018c) Report of Coordinating Committee for Prediction of Volcanic Eruption No.124. Jpn Meteorol Agency, Tokyo, Accessed 27 July 2018 https://www.data.jma.go.jp/svd/vois/data/tokyo/STOCK/kaisetsu/CCPVE/Report/ccpve_bulletin_124.html (in Japanese)

Jessop DE, Jellinek AM (2014) Effects of particle mixtures and nozzle geometry on entrainment into volcanic jets. Geophys Res Lett 41:3858–3863. https://doi.org/10.1002/2014GL060059

Johnson JB (2003) Generation and propagation of infrasonic airwaves from volcanic explosions. J Volcanol Geotherm Res 121:1–14. https://doi.org/10.1016/S0377-0273(02)00408-0

Johnson JB, Lees JM (2010) Sound produced by the rapidly inflating Santiaguito lava dome, Guatemala. Geophys Res Lett 37:L22305. https://doi.org/10.1029/2010GL045217

Johnson JB, Miller AJC (2014) Application of the monopole source to quantify explosive flux during Vulcanian explosions at Sakurajima Volcano (Japan). Seismol Res Lett 85:1163–1176. https://doi.org/10.1785/0220140058

Johnson JB, Ripepe M (2011) Volcano infrasound: a review. J Volcanol Geotherm Res 206:61–69

Johnson JB, Aster RC, Kyle PR (2004) Volcanic eruptions observed with infrasound. Geophys Res Lett 31:L14604. https://doi.org/10.1029/2004GL020020

Kato K, Yamasato H (2013) The 2011 eruptive activity of Shinmoedake volcano, Kirishimayama, Kyushu, Japan—overview of activity and volcanic alert level of the Japan Meteorological agency. Earth Planets Sp 65:489–504. https://doi.org/10.5047/eps.2013.05.009

Kim K, Lees JM, Ruiz M (2012) Acoustic multipole source model for volcanic explosions and inversion for source parameters. Geophys J Int 191:1192–1204. https://doi.org/10.1111/j.1365-246X.2012.05696.x

Kim K, Fee D, Yokoo A, Lees JM (2015) Acoustic source inversion to estimate volume flux from volcanic explosions. Geophys Res Lett 42:5243–5249. https://doi.org/10.1002/2015GL064466

Lighthill MJ (1967) Waves in fluids. Commun Pure Appl Math 20:267–293. https://doi.org/10.1002/cpa.3160200204

Marchetti E, Ripepe M, Harris AJL, Delle Donne D (2009) Tracing the differences between Vulcanian and Strombolian explosions using infrasonic and thermal radiation energy. Earth Planet Sci Lett 279:273–281. https://doi.org/10.1016/j.epsl.2009.01.004

Matoza M, Fee D, Garcés MA et al (2009) Infrasonic jet noise from volcanic eruptions. Geophys Res Lett 36:L08303. https://doi.org/10.1029/2008GL036486

Morrissey M, Garces M, Ishihara K, Iguchi M (2008) Analysis of infrasonic and seismic events related to the 1998 Vulcanian eruption at Sakurajima. J Volcanol Geotherm Res 175:315–324. https://doi.org/10.1016/j.jvolgeores.2008.03.008

Morton BR, Taylor G, Turner JS (1956) Turbulent gravitational convection from maintained and instantaneous sources. Proc R Soc A Math Phys Eng Sci 234:1–23. https://doi.org/10.1098/rspa.1956.0011

Nagaoka S, Okuno M (2011) Tephrochronology and eruptive history of Kirishima volcano in southern Japan. Quat Int 246:260–269. https://doi.org/10.1016/j.quaint.2011.06.007

Nakada S, Nagai M, Kaneko T, Suzuki Y, Maeno F (2013) The outline of the 2011 eruption at Shinmoe-dake (Kirishima), Japan. Earth Planets Space 65:475–488. https://doi.org/10.5047/eps.2013.03.016

Oshima H, Maekawa T (2001) Excitation process of infrasonic waves associated with Merapi-type pyroclastic flow as revealed by a new recording system. Geophys Res Lett 28:1099–1102. https://doi.org/10.1029/1999GL010954

Patrick MR (2007) Dynamics of Strombolian ash plumes from thermal video: motion, morphology, and air entrainment. J Geophys Res Solid Earth 112:B06202. https://doi.org/10.1029/2006JB004387

Patrick MR, Harris AJL, Ripepe M, Dehn J, Rothery DA, Calvari S (2007) Strombolian explosive styles and source conditions: insights from thermal (FLIR) video. Bull Volcanol 69:769–784. https://doi.org/10.1007/s00445-006-0107-0

Petersen T, De Angelis S, Tytgat G, McNutt SR (2006) Local infrasound observations of large ash explosions at Augustine Volcano, Alaska, during January 11-28, 2006. Geophys Res Lett 33:L12303. https://doi.org/10.1029/2006GL026491

Ripepe M, Marchetti E (2002) Array tracking of infrasonic sources at Stromboli volcano. Geophys Res Lett 29:33-1–33-4. https://doi.org/10.1029/2002GL015452

Ripepe M, Ciliberto S, Della Schiava M (2001) Time constraints for modeling source dynamics of volcanic explosions at Stromboli. J Geophys Res Solid Earth 106:8713–8727. https://doi.org/10.1029/2000JB900374

Sato E, Fukui K, Shimbori T (2018) Aso volcano eruption on October 8, 2016, observed by weather radars. Earth Planets Space 70:105. https://doi.org/10.1186/s40623-018-0879-4

Scorer RS (1957) Experiments on convection of isolated masses of buoyant fluid. J Fluid Mech 2:583–594. https://doi.org/10.1017/S0022112057000397

Shimbori T, Sakurai T, Tahara M, Fukui K (2013) Observation of eruption clouds with weather radars and meteorological satellites: a case study of the eruptions at Shinmoedake volcano in 2011. Q J Seismol 77:139–214 (in Japanese with English abstract)

Sparks RSJ, Wilson L (1976) A model for the formation of ignimbrite by gravitational column collapse. J Geol Soc Lond 132:441–451. https://doi.org/10.1144/gsjgs.132.4.0441

Sparks RSJ, Bursik MI, Carey SN, Gilbert JS, Glaze LS, Sigurdsson H, Woods AW (1997) Volcanic plumes. Wiley, London, p 574

Suzuki Y, Koyaguchi T (2015) Effects of wind on entrainment efficiency in volcanic plumes. J Geophys Res Solid Earth 120:6122–6140. https://doi.org/10.1002/2015jb012208

Terada A, Ida Y (2007) Kinematic features of isolated volcanic clouds revealed by video records. Geophys Res Lett 34:L01305. https://doi.org/10.1029/2006gl026827

Turner J (1962) The "starting plume" in neutral surroundings. J Fluid Mech 13:356–368. https://doi.org/10.1017/S0022112062000762

University of Wyoming (2017) Sounding data of upper air data. Accessed 1 December 2017 http://weather.uwyo.edu/upperair/sounding.html

Vergniolle S, Brandeis G (1994) Origin of the sound generated by Strombolian explosions. Geophys Res Lett 1:1959–1962. https://doi.org/10.1029/94GL01286

Vergniolle S, Brandeis G (1996) Strombolian explosions: 1. A large bubble breaking at the surface of a lava column as a source of sound. J Geophys Res Solid Earth 101:20433–20447. https://doi.org/10.1029/96JB01178

Vergniolle S, Caplan-Auerbach J (2004) Acoustic measurements of the 1999 basaltic eruption of Shishaldin volcano, Alaska 2. Precursor to the Subplinian phase. J Volcanol Geoth Res 137:135–151. https://doi.org/10.1016/j.jvolgeores.2004.05.004

Vergniolle S, Caplan-Auerbach J (2006) Basaltic thermals and Subplinian plumes: constraints from acoustic measurements at Shishaldin volcano, Alaska. Bull Volcanol 68:611–630. https://doi.org/10.1007/s00445-005-0035-4

Vergniolle S, Boichu M, Caplan-Auerbach J (2004) Acoustic measurements of the 1999 basaltic eruption of Shishaldin volcano, Alaska 1. Origin of Strombolian activity. J Volcanol Geoth Res 137:109–134. https://doi.org/10.1016/j.jvolgeores.2004.05.003

Vidal V, Géminard JC, Divoux T, Melo F (2006) Acoustic signal associated with the bursting of a soap film which initially closes an overpressurized cavity. European Phys J B - Condens Matter Complex Syst 54:321–339. https://doi.org/10.1140/epjb/e2006-00450-0

Wilson L, Self S (1980) Volcanic explosion clouds: density, temperature, and particle content estimates from cloud motion. J Geophys Res Solid Earth 85:2567–2572. https://doi.org/10.1029/jb085ib05p02567

Woods A, Kienle J (1994) The dynamics and thermodynamics of volcanic clouds: theory and observations from the April 15 and April 21, 1990 eruptions of redoubt volcano, Alaska. J Volcanol Geotherm Res 62:273–299. https://doi.org/10.1016/0377-0273(94)90037-X

Woulff G, McGetchin TR (1976) Acoustic noise from volcanoes: theory and experiment. Geophys J R Astron Soc 45:601–616. https://doi.org/10.1111/j.1365-246X.1976.tb06913.x

Yamada T, Aoyama H, Nishimura T, Yakiwara H, Nakamichi H, Oikawa J, Iguchi M, Hendrasto M, Suparman Y (2016) Initial phases of explosion earthquakes accompanying Vulcanian eruptions at

Lokon-Empung volcano, Indonesia. J Volcanol Geotherm Res 327: 310–321. https://doi.org/10.1016/j.jvolgeores.2016.08.011

Yamada T, Aoyama H, Nishimura T, Iguchi M, Hendrasto M (2017) Volcanic eruption volume flux estimations from very long period infrasound signals. Geophys Res Lett 44:143–151. https://doi.org/10.1002/2016GL071047

Yamamoto H, Watson IM, Phillips JC, Bluth GJ (2008) Rise dynamics and relative ash distribution in Vulcanian eruption plumes at Santiaguito Volcano, Guatemala, revealed using an ultraviolet imaging camera. Geophys Res Lett 35:L08314. https://doi.org/10.1029/2007GL032008

Yokoo A, Miyabuchi Y (2015) Eruption at the Nakadake 1st Crater of Aso volcano started in November 2014. Bull Volcanol Soc Jpn 60: 275–278 (in Japanese)

Yokoo A, Tameguri T, Iguchi M (2009) Swelling of a lava plug associated with a Vulcanian eruption at Sakurajima Volcano, Japan, as revealed by infrasound record: case study of the eruption on January 2, 2007. Bull Volcanol 71:619–630. https://doi.org/10.1007/s00445-008-0247-5

Yokoo A, Iguchi M, Tameguri T, Yamamoto K (2013) Processes prior to outbursts of Vulcanian eruption at Showa crater of Sakurajima volcano. Bull Volcanol Soc Japan 56:163–181. https://doi.org/10.18940/kazan.58.1_163